THE DETERMINATION OF THE ELECTRON DENSITY PROFILE OF THE HUMAN ERYTHROCYTE GHOST MEMBRANE BY SMALL-ANGLE X-RAY DIFFRACTION

E. H. PAPE, K. KLOTT, AND W. KREUTZ, *Institut für Biophysik und Strahlenbiologie der Universität Freiburg im Breisgau, D-78-Freiburg, West Germany*

ABSTRACT Diffraction patterns of stacked hemolyzed erythrocyte ghosts in the wet state were recorded. Three orders of a surprisingly high first-order periodicity of 600 Å were detected.

The scattering curves were evaluated by the Q-function method, including lattice distortions of the one-dimensional multilamellar system.

The resulting electron density profile of the membrane in the wet state is strongly asymmetric. It consists of an asymmetrical bilayer-type part and an excess of positive relative electron density at the inner, cytoplasmic, side of the membrane. The extension of the whole membrane profile in the wet state is 100–120 Å.

We suggest that the innermost positive density peak mainly represents the loosely bound protein components spectrin and actin, located at the cytoplasmic side of the membrane and sometimes seen as "fuzzy" material on electron micrographs.

INTRODUCTION

In the rapidly expanding area of membrane research the erythrocyte membrane is one of the most frequently investigated objects. Two main advantages are that the membrane is readily available and can be prepared without contamination of other material. A continuously increasing number of investigations in biochemistry, biophysics, and physiology characterize the exceptional position of this object.

However, in the natural state the red blood cells do not form an ordered array (like nerve myelin, chloroplast thylakoids, or retina disks); moreover, they show a very high deformability and can take a diversity of shapes. In addition, the isolation normally includes the osmotic lysis of the erythrocyte, and the membranes obtained by this procedure, hemoglobin-free ghosts, in principle can differ in their architecture from the original membranes.

On the one hand, a minimum of alteration due to the preparation procedure is

---

Dr. Klott's present address is: Medizinisches Strahleninstitut, University of Tübingen, D-74 Tübingen, W. Germany.

desired. On the other hand, certain preparative operations are obviously necessary to get a sufficiently well ordered system for a structural investigation.

Previous attempts to elucidate the structure, especially the density profile of the erythrocyte membrane by X-ray diffraction should be briefly mentioned.

Husson and Luzzati (1963) have especially studied the effect of saponin treatment of ghosts, and for lyophilized ghosts untreated with saponin they have found a diffraction pattern consisting of three orders of a periodicity of 170–205 Å, dependent on the temperature (22°C–37°C, respectively).

Finean and co-workers have investigated erythrocyte ghosts of rats and of human blood in a variety of conditions (Finean et al., 1966, 1968; Knutton et al., 1970; Finean, 1972).

From erythrocyte ghosts prepared at very low osmolarities they have recorded four diffraction orders related to a periodicity between 100 and 120 Å ("Type I" membranes). In comparison with simultaneous electron microscope observations they concluded that this distance might be the single membrane period. The fact that only the second, fourth, and sixth order of the double membrane period were recorded indicates that the density profile of the membrane must be nearly symmetrical at this preparative state.

Wilkins et al. (1971) have studied erythrocyte ghost membranes in the form of dispersions, not in regular arrays. They came to the conclusion that a lipid bilayer with an extension of 45 Å must be a structural element of the membrane.

Recently Stamatoff et al. (1975) came to the result that the electron density profile of the ghost membrane should have an extension of only 55 Å. This latter finding has been called in question by Blaurock and Lieb (1975) in a comment, in which they assumed, from the great similarity between the membrane electron density profile and the profile of a bimolecular lipid bilayer, that the density profile very probably must be related to a separate lipid phase.

Finean et al. (1975) came to the same conclusions. They reported the appearance of a reflection corresponding to a periodicity between 200 and 300 Å (225 Å), which they had not observed in earlier investigations. This reflection is related to the double membrane period and its appearance is a precondition for obtaining an asymmetrical electron density profile.

In our experiments we have recorded a surprisingly high first-order reflection (600 Å), comparable with diffraction patterns of swollen membrane systems. In this case, a straightforward analysis of the scattering curves is possible. Additionally, it is shown that the quantitative consideration of lattice distortions is indeed necessary.

METHODS

Preparation of the Erythrocyte Ghosts

Ghosts from human blood were prepared by a modification of the method of Dodge et al. (1963) through hemolysis in hypotonic medium. 10 ml human blood (conserve Biopack-acid citrate dextrose with adenine from the local blood bank) group O Rh^+, were centrifuged for 10 min at

3,000 *g*; the plasma and the buffy coat were removed. The erythrocytes were then washed four times in isotonic Ringer solution.

The hemolysis was performed by incubation of each 2 ml of erythrocytes in 40 ml phosphate buffer (20 mosmol, pH 8.0) for 30 min.

After a subsequent centrifugation at 25,000 *g* for 15 min, the hemolysate was discarded. The pellet was again resuspended in phosphate buffer (20 mosmol) and after washing according to the method of Dodge et al. (1963) and a final washing in Tris-EDTA-buffer-solution (10 mosmol Tris, 1 mM EDTA), nearly hemoglobin-free ghosts were obtained (remaining Hb concentration < 0.2% of mean corpuscular hemoglobin content).

The effect of the inclusion of EDTA into the washing solution after hypertonic hemolysis has been studied in detail by Bramley and Coleman (1972). They found in the presence of 1 mM EDTA a strong dependence on the osmolarity: at 40 mosmol phosphate buffer (pH 7.4) the ghosts are more "flexible" and highly suitable for many studies. On the contrary, at 5 mosmol Tris-NaCl buffer (pH 7.4), the ghosts showed a greater tendency to fragment into vesicles.

The conditions for our preparations were chosen to get a minimal Hb value and to preserve structural integrity. The latter can be seen in the electron micrograph of Fig. 2. The following storage of the ghosts in a hypertonic solution (12% sorbite = 660 mosmol) corresponds to conditions that prevent vesiculation of the ghosts. However, it cannot be completely excluded that part of the nonhemoglobin protein is also removed from the membrane.

The pellet then was resuspended in a 12%-sorbite-Tris-EDTA solution (12 *g* sorbite in 100 ml Tris-EDTA buffer) and was centrifuged 60 min at 150,000 *g* in a Beckman Spinco L 50, Titan rotor SW 50.1 (Beckman Instruments, Inc., Spinco Div., Palo Alto, Calif.). The addition of sorbite, known to stabilize the morphology of erythrocytes (Schneider et al., 1972) was necessary to get a sufficiently well-ordered stacking system of wet ghosts. The ghosts were prepared at 4°C. The diffraction experiments were performed at room temperature (25°C).

X-ray Diffraction Patterns

WET GHOSTS A sample of the very viscous ghost pellet was placed on the gap in a small lead ring in accordance with the technique of Finean et al. (1966). The sample holder was then placed in a Kratky cuvette. A stream of nitrogen that first passed a water bath warmer than room temperature (37°C) prevented dehydration of the sample. A subsequent humidity controller showed a relative humidity of 100%. By this technique surprisingly high periods of the lamellar repeat were detectable. An example, using line collimation, is presented in Fig. 1.

The pattern consists of three orders of a periodicity of 600 Å and two broad maxima centered at angles that correspond to Bragg spacings of 110 and 66 Å. The latter broad scattering maxima represent the pure structure factor of a double membrane. They are oriented in the same way as the maxima of the lattice factor.

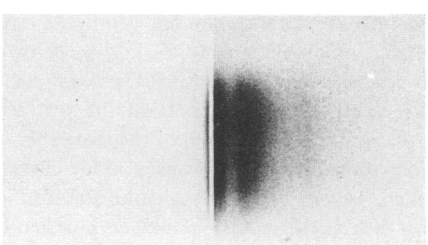

FIGURE 1 X-ray diffraction pattern of stacked erythrocyte ghosts in the wet state (exposure time 48 h, Kratky camera, crystal-monochromatized Cu-K_α-radiation, sample-to-film distance 242 mm).

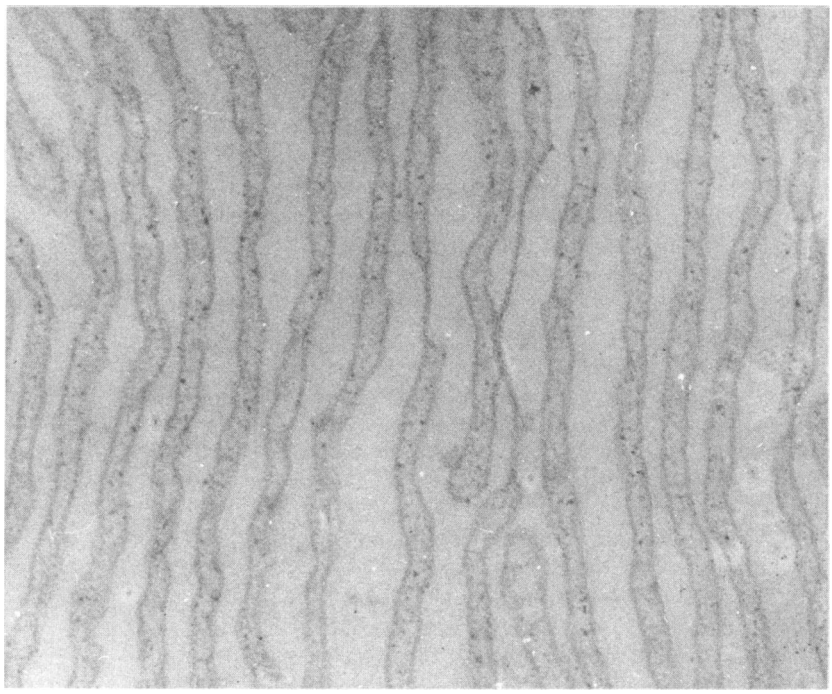

FIGURE 2 Thin section of stacked erythrocyte ghosts (wet state) after the diffraction experiment (by J. Fritz and B. Hildmann) fixed in glutaraldehyde (45 min) and OsO_4 (3 h), embedded in Araldite, stained with uranyl acetate and lead citrate), magnification 100,000.

An electron micrograph, taken after the X-ray exposure of the specimen, is shown in Fig. 2. The large period of the X-ray diffraction experiment is confirmed (the average stacking period is ~650 Å) and, secondly, the inner space of the ghosts appears more electron dense than the outer space between the stacked ghosts.

The observation that the interspace between adjacent ghosts is larger than or equal to the double membrane extension (ghost thickness) is of particular importance in the following evaluation.

To control the influence of the disorientation of the ghosts in the X-ray scattering experiment, in addition an exposure series using pinhole geometry was performed. For this purpose limiting slits are introduced into the Kratky camera geometry. A photograph of this series is seen in Fig. 3. On the short time exposure (5 h, Fig. 3, below), three orders of the long periodicity 600 Å are clearly resolved (see also the corresponding densitometer curve (Fig. 5).

On the long time exposure (72 h), the outer part of the scattering curve can be recorded. The medium time exposure allows the combination of the two other curves (Fig. 5, right side).

The main additional information taken from these pinhole curves is the degree of disorientation of the regions of stacked ghosts. The half angle of disorientation was 30°.

Assuming a distribution of different orientations like a Gaussian (normal distribution) about the preferred axis, it is possible to correct the line-smeared curve with respect to this special collimation effect.

Details of this slit height correction, which depends on the arc (or sickle) of the disorientation, are given in Appendix C.

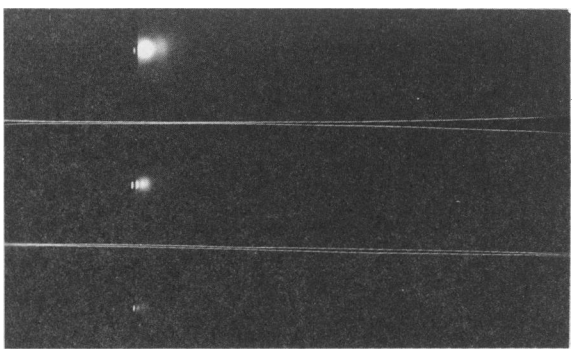

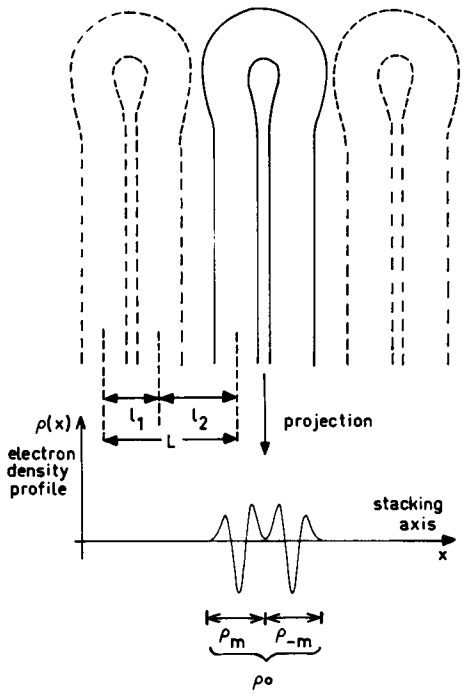

FIGURE 3

FIGURE 4

FIGURE 3 Sequence of small angle X-ray diffraction pattern with increasing exposure time with a point-focused X-ray beam. The exposure times are: top, 72 h, middle, 24 h, below, 5 h. Ni-filtered Cu-K_α radiation, sample-to-film distance 250 mm.

FIGURE 4 Schematic representation of the scattering system.

The X-ray patterns were recorded on Agfa Structurix D10 films (Agfa-Gevaert Inc., Leverkusen, W. Germany) with a Kratky-camera (Figs. 1 and 3) manufactured by Fa.Anton Paar, Graz, Austria. The densitometer tracings were obtained on a microdensitometer model MK III C (Joyce, Loebl and Co., Ltd., Gateshead-on-Tyne, England).

Evaluation of the Scattering Intensity Curves

THE EVALUATION METHOD We apply the deconvolution or Q function method of Hosemann and Bagchi (1962). Additionally we take lattice distortions into account, described by distance distribution functions between neighboring membranes.

The principle of the Q function method should be remembered: A Fourier transformation of the scattered intensity function yields the Q function, and a deconvolution of the isolated Q_0 function gives us the electron density distribution (EDD) of the unit cell. The Q function method is applicable if the Q_0 function, the generalized Patterson function of one unit cell, is separable. This is possible in two cases: (*a*) The crystal or scattering system contains only a small number of unit cells. The corresponding Q function is a rapidly decreasing quasi-periodic function from which the Q_0 function can be isolated. Examples are given by Kreutz (1968, 1970) and by Lesslauer et al. (1971, 1972). (*b*) In certain cases of swollen biological membrane systems, characterized by a region of constant electron density between consecutive unit cells, this level can be considered as level of zero relative electron density.

In such a case the Q function is obtained without an additional separation procedure. If the extension of the swelling zone exceeds the extension of the double membrane, the repeating terms of $Q(x)$, which are centered at the lattice points nL, do not overlap each other. Examples for the latter case are given by McIntosh and Worthington (1974) and Worthington and McIntosh (1974) in the case of swollen nerve myelin.

However, multilayers of biological membranes, *in situ* as well as artificially prepared, cannot be considered as perfectly ordered systems like ideal one-dimensional crystals. On the contrary, a certain degree of disorder will remain, even in such well-ordered systems as nerve myelin (Blaurock and Nelander, 1976).

The influence of lattice distortions on the Q function is generally discussed in the books of Hosemann and Bagchi (1962) and Vainshtein (1966), by Schwartz et al. (1975), and by Kreutz and Pape (1975). Our evaluation procedure, which includes the consideration of lattice distortions, will be presented in the following.

The multilayer can be described by a one-dimensional system with a regular sequence of image and mirror-image of the single membrane profile ρ_m (Fig. 4). Let $\rho(x)$ represent the projected EDD onto the stacking axis x. $\rho_0(x)$ denotes the projected EDD of a unit cell (double membrane), which consists of the EDD of a single membrane $\rho_m(x)$ and in a spacing of l_1 from it the EDD of its mirror image $\rho_{-m}(x) = \rho_m(-x)$:

$$\rho_0(x) = \rho_m(x) + \rho_{-m}(x) * \delta(x - l_1). \tag{1}$$

We distinguish between l_1, the *intra*-unit cell nearest neighbor distance, and l_2, the *inter*-unit cell nearest neighbor distance of neighboring single membranes (see Fig. 4).

Let us further introduce the function $H_1(x)$and $H_2(x)$, each of them describing a statistical distance distribution function between neighboring membranes. $H_1(x)$ is related to the intra-unit cell distance l_1, and $H_2(x)$ to the inter-unit cell distance l_2.

The following notations are used: $*$, convolution symbol defined by:

$$[f * g](x) = \int_{-\infty}^{+\infty} f(t)g(x - t)\,dt;$$

$$Q_m = \rho_m * \rho_{-m}; \quad Q_{m1} = \rho_m * \rho_m; \quad Q_{m2} = \rho_{-m} * \rho_{-m};$$

$\delta(x)$ = Dirac's delta function symbol; N = number of unit cells within a multilayer.

In the following, only the right half of the always centro-symmetrical functions $Q(x)$ and $Q_0(x)$ is represented. The Q_0 function, the convolution $\rho_0(x)$ with $\rho_0(-x)$, the generalized Patterson function of the unit cell, is given in these terms by:

$$Q_0(x) = 2Q_m(x) * \delta(x - 0) + Q_{m2}(x) * H_1(x); \quad x \geq 0. \tag{2}$$

This equation degenerates in the absence of distortions ($H_1(x)$ becomes pointlike) to:

$$Q_0(x) = 2Q_m(x) * \delta(x - 0) + Q_{m2}(x) * \delta(x - l_1); \quad x \geq 0. \tag{2a}$$

The complete Q-function of a multilayer of N unit cells is then:

$$\begin{aligned} Q(x) = {} & N[2Q_m(x) * \delta(x - 0) + Q_{m2}(x) * H_1(x)] \\ & + x \geq 0 + (N - 1)[Q_{m1} * H_2 + 2Q_m * H_1 * H_2 + Q_{m2} * H_1 * (H_1 * H_2)] \\ & + \sum_{n=2}^{N-1} (N - n)[Q_{m1} * H_2 + 2Q_m * H_1 * H_2 + Q_{m2} * H_1 * (H_1 * H_2)] \\ & * [H_1 * H_2]_{n-1} \end{aligned} \tag{3}$$

where

$$[H_1 * H_2]_n = \overbrace{[H_1 * H_2] * [H_1 * H_2] * \cdots\cdots * [H_1 * H_2]}^{n\text{-times}}$$

Details of the calculation are given in Appendix A.

The effect of disorder in the one-dimensional arrangement can be characterized by the following points: (*a*) The inner part, $2Q_m$, convoluted with a delta function at the origin, is not altered and becomes the predominant part of Q. It represents the convolutions of the membrane profiles with "itself." (*b*) The decrease of $Q(x)$ with increasing x is caused by the convolution of the corresponding parts of $Q(x)$ with the distance statistic functions H_1 and H_2 and their convolution polynomials, depending on the widths of H_1 and H_2 and on the number N of the unit cells within a multilayer.

If the extension of the interspace is larger than the double membrane thickness, then the Q_0 function centered at the origin does not overlap the outer terms of the Q function.

In the case of wet erythrocyte ghost membranes ($L = l_1 + l_2 = 600$ Å, double membrane thickness <300 Å), the condition for such an isolated Q_0 function is realized and we can use Eq. 2 in the determination of $\rho_o(x)$.

Gaussian Deconvolution Method Including Distance Distributions

To calculate the electron density profile $\rho_m(x)$ of a single membrane from the experimentally obtained Q function by a deconvolution process, we proceed in the following way: We represent the electron profile ρ_m by a sum of N Gaussians of the same width:

$$\rho_m(x) = \sum_{i=1}^{N} A_i \exp[-c(x - x_i)^2]. \tag{4}$$

We generate $H(x)$, also by a Gaussian. It is convenient to choose Gaussian functions, because the convolution of a Gaussian with a Gaussian is again a Gaussian function. Thus, all terms in Eqs. 2 and 3 are easily calculated as convolution polynomials of Gaussian functions. Details are given in Appendix A.

It has been tested that an introduction of Gaussians of different width in ρ_m has no significant effect on the degree of agreement between experimentally observed and synthetized functions. It merely increases the number of parameters, which is not desired.

At first starting with an initial set of parameters A_i, x_i, c for ρ_m, we calculate the quantities Q_m, Q_{m2}, Q_{m1} and, using H_1 and H_2 (if necessary), the complete expression $Q_0(x)$ according to Eq. 2 or $Q(x)$ according to Eq. 3. The result is compared with the experimentally obtained function Q_{exp}, calculated by an inverse Fourier transformation of the scattered intensity. In a subsequent least-square refinement procedure (Marquardt, 1963), the parameters of the model ρ_m are varied until the squared differences between Q_{mod} and Q_{exp} are minimized. The solution ρ_m that gives the best agreement between Q_{mod} and Q_{exp} will be considered as the correct one.

Tests of Validity

REMOVAL OF THE DISTANCE DISTRIBUTION FUNCTION $H_1(x)$ When the distance distribution function H_1 is determined, namely the mean distance l_1 and the half-width $2x_n = (ln\ 2/c_1)^{1/2}$, we can "sharpen" the Q_0 function by replacing $H_1(x)$ by a pointlike function, localized at the same distance l_1 (see also Eq. 2*a*). In this way we get the undistorted Q_0 func-

tion of a structure with a center of symmetry. Such a Q_0 function has an unambiguous solution (deconvolution root) ρ_0, except for the reflection about the abscissa, $-\rho_0$ (Hosemann and Bagchi, 1962, p. 121).

Thus, we can apply the Fourier analytical deconvolution method (FAD method) (Pape, 1974), a direct method without iterations.

COMPARISON OF $F_0^2(b)$ AND $\overline{F_0^2}(b)$ WITH THE EXPERIMENTALLY OBTAINED INTENSITY FUNCTION $I_{exp}(b)$ We evaluate the scattered intensity diagrams by the Q function method because we are first interested in the structure of the unit cell ρ_0 and not until then in the mutual arrangement of the unit cells, that is, in the lattice structure. A separation of these two types of structure can be better performed in the Q function representation than in the intensity representation. However, as a control of our results, we calculate the corresponding structure factor $F_0^2(b)$ of the $\rho_0(x)$, found by the Q-function method, then the averaged structure factor $\overline{F_0^2}(b)$, and compare it with the experimental intensity curve. F_0 is given by a Fourier transformation of $\rho_0(x)$

$$F_0(b) = \int_{-\infty}^{+\infty} \rho_0(x) \exp(2\pi i b x)\, dx \tag{5}$$

$\overline{F_0^2}$ is the result of averaging of F_0^2 according to the distance distribution function $H_1(x)$. Details are given in Appendix B.

RESULTS

In Fig. 5 the densitometer curves of the sample scattering and the background scattering corresponding to the "point" collimation experiments are represented. Exposure times are indicated at the corresponding scattering curves.

The densitometer tracings referring to the slit-smeared pattern are seen in Fig. 6*a*. The exposure time was 48 h. The smoothed intensity curve and the reference curve, consisting of the background scattering of the camera and the specimen holder, also exposed 48 h, are drawn in Fig. 6*b*. Comparing the two scattering curves in Figs. 5 and 6, we clearly see that the decrease of the experimentally observed intensity is faster in the case of pinhole geometry.

The influence of the background subtraction on the final results is investigated in a separate part at the end of this section.

In Fig. 7 the result of the special height-desmearing correction (see Appendix C), applied to the slit-smeared curve (Fig. 6) is presented. After the desmearing, the appropriate Lorentz correction was performed by a multiplication by b^2.

In Fig. 8, the desmeared line collimation curve and the pinhole curve, both Lorentz-corrected, are compared with each other. Their corresponding Q functions, obtained by a Fourier *cos*-transformation, are represented in Fig. 9.

Again there are no great differences between the two curves. The following evaluation starts from Q_l, the Q function referred to the desmeared line collimation intensity curve. (It should be mentioned that alternative calculations starting from the Q function, corresponding to the pinhole intensity curve, led to the same final results within the margin of error.)

It is remarkable that the oscillations in $Q_{exp}(x)$ practically vanish outside an interval of $0 \leq x \leq 300$ Å. The expected peak at $x = 600$ Å is observed but has a very

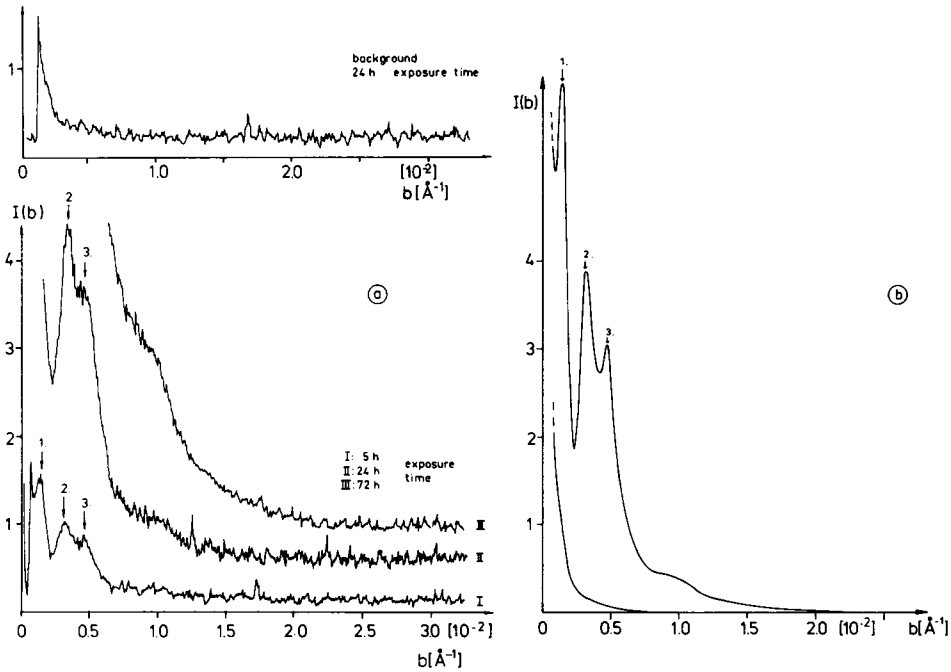

FIGURE 5 Densitometer tracings (*a*) and smoothed densitometer curves (*b*) corresponding to the sequence of point-collimated diffraction patterns of wet ghosts (see Fig. 3) and the appropriate background curve.

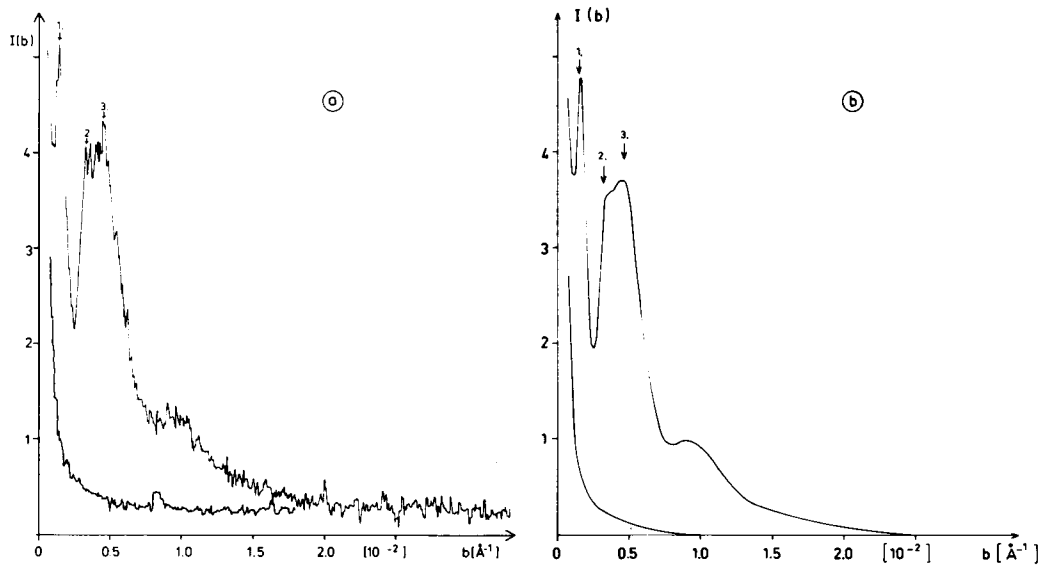

FIGURE 6 Densitometer tracings (*a*) and smoothed densitometer curves (*b*) corresponding to the line-collimated diffraction pattern of wet ghosts (see Fig. 1) and the appropriate background curve.

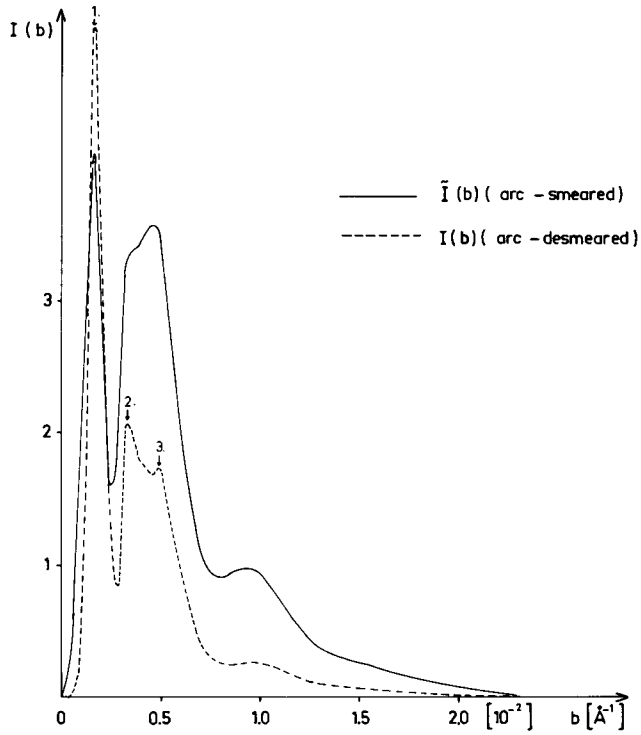

FIGURE 7 Result of the beam height collimation correction (Appendix C) applied to the scattering curve of Fig. 6*b*.

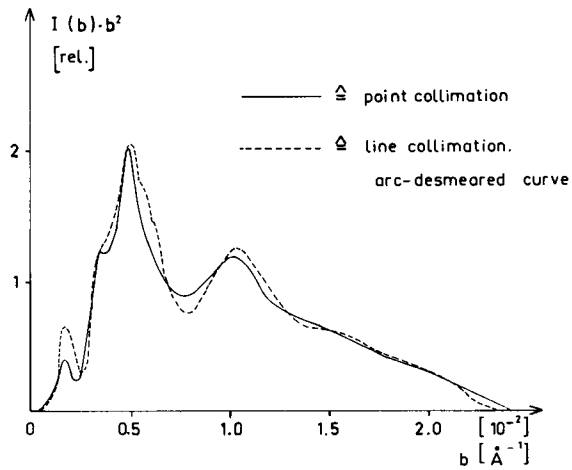

FIGURE 8 Comparison of the scattering curves of wet ghosts using different collimation geometry of the X-ray beam; both curves are Lorentz-corrected by multiplication by a factor b^2. (——) corresponds to the point-collimated pattern (Fig. 5); (- - -) slit height corrected (arc-desmeared) curve, obtained from the line-collimated pattern (Fig. 6).

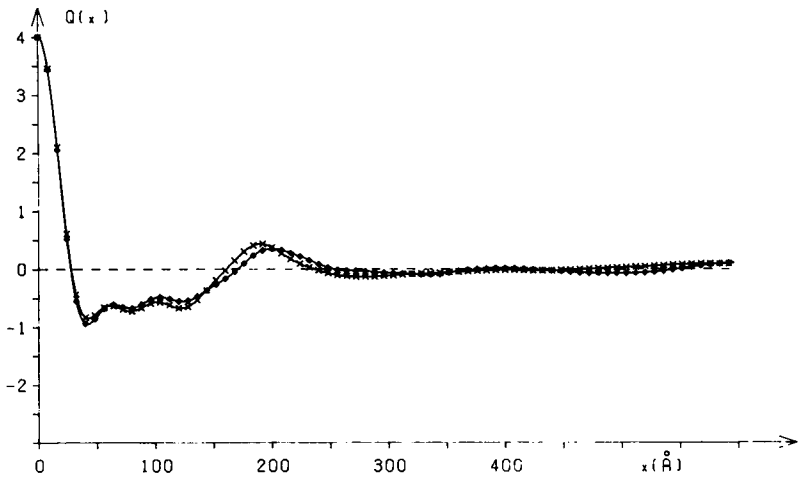

FIGURE 9 Experimental Q function of wet ghosts, obtained by a Fourier-cos transformation of the corrected experimental intensity curve. ++++, using corrected line collimation data. ♦, using point collimation data.

low amplitude. The Q function is then deconvoluted according to the least square Gaussian deconvolution method described above, with Eq. 2.

Two different parameter sets are optimized: (*a*) ρ_m is built up by a sum of three Gaussians, and $H_1(x)$ is symmetrical (Fig. 10*a*); (*b*) ρ_m is composed of four Gaussians, and $H_1(x)$ is symmetrical (Fig. 10*b*).

Moreover, a model ρ_m composed of five Gaussians was used in the deconvolution procedure, but the result was the same as with four Gaussians.

The Q function of the models, Q_{mod}, was calculated in the interval of $0 \leq x \leq 300$ Å for an Δx of 2 Å in a sufficiently brief computing time (~ seven iterations in 1 min).

To measure the reliability we define the quantity R_Q

$$R_Q = \frac{\Sigma[Q_{\text{exp}}(x_i) - Q_{\text{mod}}(x_i)]^2}{\Sigma[Q_{\text{exp}}(x_i)]^2}. \tag{6}$$

The "best" values of the parameters A_k, x_k, c, c_1, l_1 and the corresponding R_Q values are listed in Table I. In a second optimization procedure, the region of the fit was extended to the interval of $0 \leq x \leq 600$ Å, with the first four terms of Eq. 3. The resulting values of the parameters are listed in Table II.

A comparison of the corresponding R_Q values clearly favors the four-Gaussian model. We consider this model with the lowest R_Q value as the correct one at the given low resolution.

The parameters A_k, x_k, and c in Table II, describing the density profile ρ_m, are almost the same as in Table I. A value of $\frac{5}{6}$ was chosen for the quantity $(N - 1)/N$.

The first test of reliability, the removal of the distance statistics H_1 from the four-Gaussian best parameter set, leads to the sharpened Q_0 function, seen in Fig. 11. The

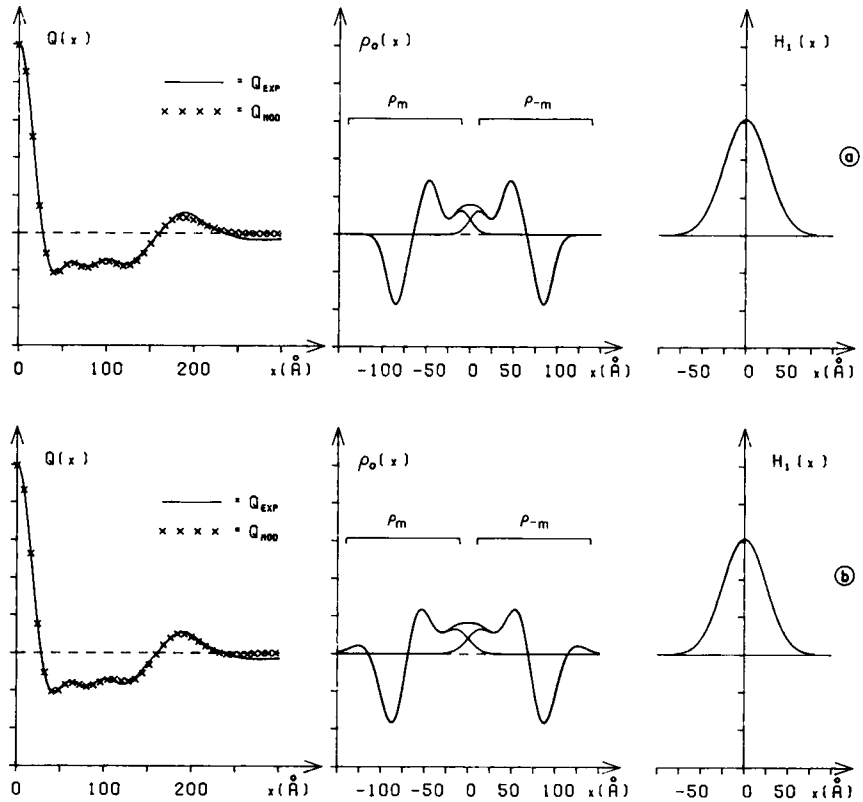

FIGURE 10 Deconvolution of the Q_0 function (wet ghosts) by the least-square Gaussian deconvolution method. (*a*), the model ρ_m is composed of three Gaussians; (*b*), the model ρ_m is composed of four Gaussians. All ordinates are in relative units.

result of the direct deconvolution by the FAD method (Pape, 1974) is seen on the right side of Fig. 11. The recalculated convolution square of the solution ρ_0, Q_{SHR}, is also drawn in Fig. 11 and agrees well with Q_{SH}. The results of the second test of reliability, the comparison of the reconstructed F_0^2 and $\overline{F_0^2}$ with the experimental, desmeared, and Lorentz-corrected intensity $I(b)\cdot b^2$, using the parameter sets of Table I and applying Eq. 15 of Appendix B, are shown in Fig. 12.

The effect of the distance statistics H_1 on F_0^2 is clearly demonstrated by a damping and smearing of the peaks of F_0^2. Again, in the case of the four-Gaussian model of ρ_m, the agreement between $\overline{F_0^2}$ and the corrected experimental intensity curve is better.

Influence of Background Correction

Generally it is difficult to measure a background curve under exactly the same experimental conditions in the case of densely packed systems. Although we have determined the appropriate reference curve, consisting of the background scattering of the

TABLE I

"BEST" VALUES OF THE PARAMETERS DESCRIBING THE MODEL DENSITY PROFILE $\rho_m(A_k, x_k, c)$ AND THE DISTANCE STATISTICS (c_1, l_1), FOUND BY THE LEAST-SQUARE GAUSSIAN DECONVOLUTION METHOD

Type of model	k	A_k	x_k	c	c_i, l_i, R_Q
			Å		
Three Gaussians	1	−1.25	0.0	0.0044	c_1 = 0.0008
	2	0.96	37.9		l_1 = 169.3 Å
	3	0.41	74.6		R_Q = 0.0049
Four Gaussians	1	0.19	−35.0	0.0023	c_1 = 0.0008
	2	−1.42	0.0		l_1 = 169.2 Å
	3	0.99	25.7		
	4	0.43	70.8		R_Q = 0.0033

The R_Q values indicate the degree of agreement between Q_{exp} and Q_{mod}. Generation of Q_{mod} in the range ($0 \leq x \leq 300$Å) is according to Eq. 2.

camera and the sample holder, the effect of the sample absorption, for example, cannot be simulated quantitatively. This is only possible in highly diluted systems.

To control the influence of the background subtraction, we performed two further evaluations using different background curves. The results are represented in Fig. 13. No significant differences in the resulting electron density profiles occur. However, the differences may serve as a margin of error in $\rho(x)$.

DISCUSSION

A general restriction is given through the low resolution of the diffraction pattern (~25 Å). Therefore, it is plausible that a model ρ_m consisting of only four Gaussians can produce sufficient details to reconstruct the observed diffraction pattern.

The diversity of solutions is strongly reduced by the fact that the double membranes (unit cells) are separated from each other by interspaces of approximately the same

TABLE II

"BEST" VALUES OF THE PARAMETERS, FOUND BY THE LEAST SQUARE GAUSSIAN DECONVOLUTION PROCEDURE

Type of model	k	A_k	x_k	$c, c_1, c_2, l_1, l_2, R_Q$	
			Å		
Three Gaussians	1	−1.24	0.0	c = 0.0044	l_1 = 169.2 Å
	2	0.97	37.8	c_1 = 0.0008	l_2 = 359.5 Å
	3	0.41	74.7	c_2 = 0.00004	R_Q = 0.0049
Four Gaussians	1	0.19	−35.0	c = 0.0023	l_1 = 168.6 Å
	2	−1.46	0.0	c_1 = 0.0008	l_2 = 367.7 Å
	3	1.05	24.9	c_2 = 0.00004	
	4	0.42	70.7		R_Q = 0.0033

In contrast to Table I, Q_{mod} is generated in the range $0 \leq x \leq 600$ A by using Eq. 3.

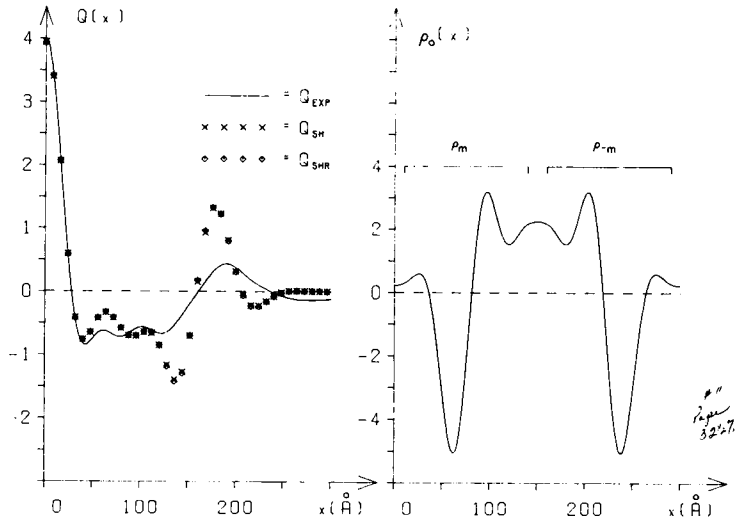

FIGURE 11 Deconvolution of the "sharpened" Q_0 function of wet ghosts by applying a direct deconvolution method (FAD method).

extension (double membrane plus interspace ~600 Å; double membrane extension alone ~300 Å).

In such a case the Q_0 function, the generalized Patterson function of one unit cell, is isolated. Our result will be the correct electron density profile (unique solution) if we can separate the undistorted Q_0 function of a structure with centrosymmetry.

Regarding Eq. 2, we see that the main problem lies in the removal of the distance distribution function $H_1(x)$. The condition for the possibility of sharpening the Q_0 function is that the term $Q_2 * H_1$ in Eq. 2 must be observable, i.e. it is necessary that the term be not completely smeared out.

In general it is not expected that only one solution ρ_m will satisfy Eq. 2 for an experimental Q_0 function. However, in the preceding case we can elucidate the situation by regarding the following points. Denoting the single membrane extension by w and the double membrane extension by $d_e \geq 2w$, then the first term $2Q_m$ has values different from zero only in the interval $(0, w)$, where it clearly dominates with respect to the second term. In the interval (w, d_e) only the second term $Q_2 * H_1$ exists, but this domain is not sufficiently well defined to get a solution by an iterative method. Moreover, the details of Q_{m2} will be more or less smeared out by the convolution with the function H_1.

However, we can extrapolate the second term towards the inner interval $(0, w)$ rather accurately, and after subtracting it from the complete Q_0 function we have both terms of Eq. 2 isolated.

Now we proceed in a way quite similar to the case of spherical bacterial thylakoids (Pape et al., 1974, Weick, 1974), where the autocorrelation function of ρ_m and the smeared convolution product were also recognized distinct from each other.

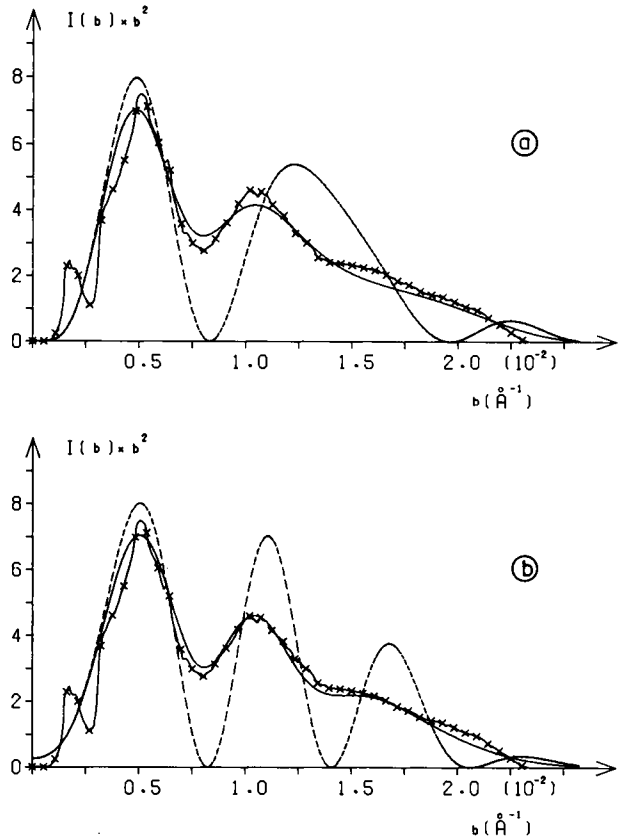

FIGURE 12 Comparison of F_0^2 (- - -), $\overline{F_0^2}$ (——) and $I(b)\cdot b^2$(xxx), using the data of Table I. (*a*) ρ_m composed of three Gaussians (see Fig. 10*a*); (*b*) ρ_m composed of four Gaussians (see Fig. 10*b*).

Systematically, we then try to find all the solutions ρ_m of the first part, $2\overset{2}{\rho}_m = 2Q_m$. Secondly we have to calculate for each solution $\rho_m * \rho_m$, fold it with a suitably chosen distance statistics $H_1(x)$, vary its width and position, and compare the result with the experimentally obtained and isolated second part of $Q_0(x)$. Only the solutions ρ_m that also generate the second part of $Q_0(x)_{exp}$ with the satisfying accuracy will remain.

In our case the remaining solutions have been the Gaussian sequence (++−+), and its mirror image (−−+−), from inside to outside. The solution $+\rho_m$ is represented in Fig. 14. We discriminate the solution $-\rho_m$, in a purely mathematical sense also possible, with regard to other biophysical and biochemical information needed to interpret the resulting electron density profile.

At first, the swelling occurs in the inter-ghost or extracellular space caused by the hypertonicity of the medium (12% sorbite corresponds to a molarity of ca. 660 mosmol, compared with the molarity of 310 mosmol of an isotonic solution. The isotonicity of erythrocytes and ghosts can differ but the above value seems to us a realistic

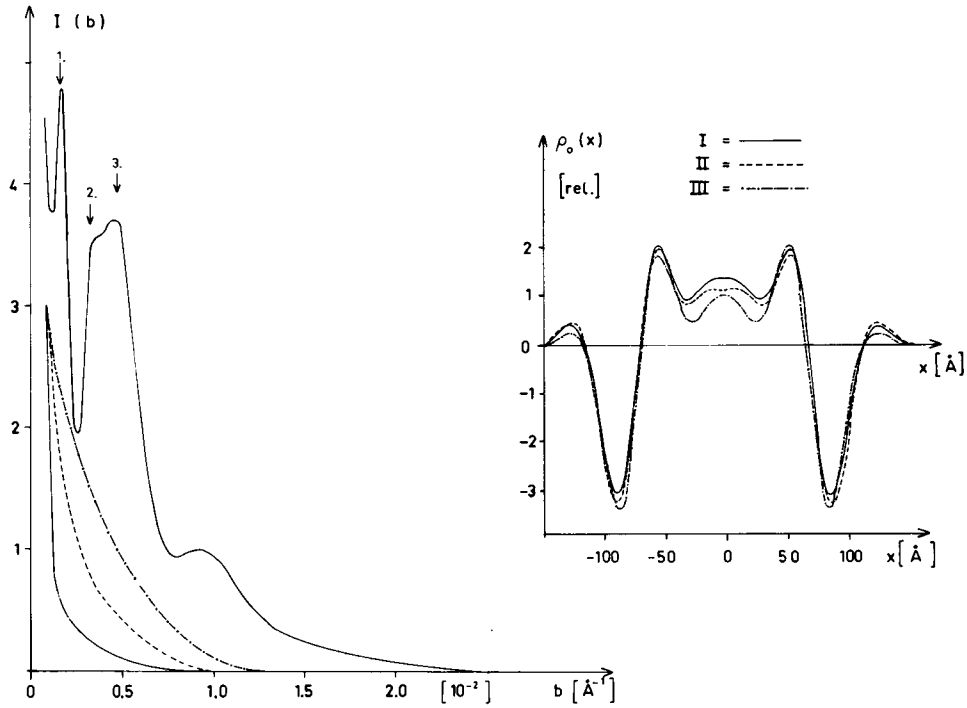

FIGURE 13 Three evaluations of the desmeared intensity curve using different background subtractions.

estimation). The electron micrograph (Fig. 2) in addition supports the choice of *one* ghost as unit cell and *not*—as an alternative—two juxtaposed membranes of neighboring ghosts.

Regarding the low resolution of the diffraction pattern, we restrict our interpretation to the following points: The first three Gaussians (from outside to inside) with a sign sequence of heights of (+ − +) represent the so-called "tripartite" structure of a lipid bilayer-containing membrane. The zone of lowest density corresponds thereby to the hydrophobic part of the membrane. The peaks of higher density in the tripartite structure are related to the lipid polar groups and to the proteins on both sides. The asymmetric arrangement of both constituents (proteins and lipids) is beyond question, especially with respect to the extrinsic proteins spectrin and actin. These components have been made visible as fuzzy material at the cytoplasmic side on electron micrographs of Tilney and Detmers (1975) and McMillan and Luftig (1975). Its amount of the total protein content is 30% (spectrin) and 4.5% (actin) (Steck, 1974). The positive peaks of the density profile on the inner side are interpreted to represent this protein excess on the cytoplasmic side of the membrane.

The possibility that sorbite contributes to the inner positive peaks is very improbable, because of the osmotic behavior of the ghosts in the sorbite-Tris-EDTA buffer as discussed above, but cannot be completely excluded.

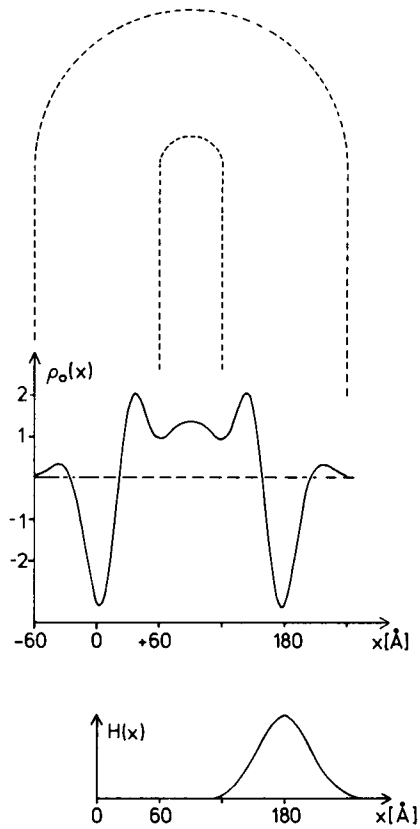

FIGURE 14 Resulting relative electron density profile of a flattened ghost. The neighboring interspaces on each side (not drawn) have almost the same extension.

The asymmetry of the electron density profile of the single membrane is not only caused by the asymmetrical distribution of the proteins but may be also influenced by the asymmetry in the arrangement of lipids within the erythrocyte membrane—monolayers of phosphatidylcholine and sphingomyelin on the outer side, monolayers of phosphatidylethanolamine and phosphatidylserine on the inner side—which is assumed on the basis of spin-label experiments (Bretscher, 1973) and treatments with phospholipases (Zwaal et al., 1973).

We are grateful to Mrs. Sophia El-Deeb, Mrs. Gerlinde Heppeler, and Mrs. Vera Müller for their excellent technical assistance. We would also like to thank Mrs. Walburga Herbst for her assistance in the preparation of the manuscript.

This work was supported in part by the Deutsche Forschungsgemeinschaft, Sonderforschungsbereich 46. The computer calculations were performed on the Univac 1106 at the Rechenzentrum of the University of Freiburg im Breisgau.

Received for publication 9 August 1976 and in revised form 22 April 1977.

APPENDIX A

Q-function of a Distorted One-dimensional Multi-Lamellar System with a Regular Sequence of Image $\rho_m(x)$ and Mirror Image $\rho_m(-x)$ within the Leaflet

In contrast to the conventional attempts (see, for instance, Vainshtein, 1966, p. 216) we have two different nearest neighbor spacings, which are allowed to vary, namely the intra-unit cell spacing l_1 and the inter-unit cell spacing l_2, between single membranes. Each of these distances may be governed by distance distribution functions (H_1 and H_2, respectively). The probability of finding the nth neighbor is given by an alternating folding of the statistics H_1 and H_2, in the sum $(n-1)$-times (lattice distortions of the second kind).

Using the same abbreviations as before, $*$ = convolution symbol, defined by:

$$[f * g](x) = \int_{-\infty}^{+\infty} f(t)g(x-t)\,dt;$$

$$Q_m = \rho_m * \rho_{-m}; \quad Q_{m1} = \rho_m * \rho_m; \quad Q_{m2} = \rho_{-m} * \rho_{-m}$$

we obtain

$$Q(x) = N \cdot (\mathrm{I}) + (N-1);(\mathrm{II}) + \sum_{n=2}^{N-1} (N-n) \cdot (\mathrm{II}) * [H_1 * H_2]_{n-1}; \quad x \geq 0 \quad (7)$$

where (I), (II), and $(H_1 * H_2)_n$ are given by (I) $= 2Q_m * \delta(x-0) + Q_{m2} * H_1$; (II) $= Q_{m1} * H_2 + 2Q_m * H_1 * H_2 + Q_{m2} * H_1 * H_2 * H_1$; $(H_1 * H_2)_n$ = nth convolution product of $(H_1 * H_2)$, and N = number of unit cells within a multilayer.

We emphasize that our description differs from that of Schwartz et al. (1975). Their distinction between lattice disorder and substitutional disorder with no correlation between them characterizes a more specialized case.

Calculation of Q_m, Q_{m1}, Q_{m2}, etc., as Convolution Polynomials of Gaussian Functions

Representing ρ_m and H_1 by

$$\rho_m(x) = \sum_{i=1}^{N} A_i \exp[-c(x-x_i)^2], \quad \text{and} \quad (8)$$

$$H_1(x) = w_1 \exp[-c_1(x-l_1)^2], \quad (9)$$

where $w_1 = (c_1/\pi)^{0.5}$, and using the formula of the convolution of two Gaussians

$$(f_i = A_i \exp[-c_i(x-x_i)^2]$$

with each other:

$$f_1 * f_2 = \int_{-\infty}^{+\infty} f_1(t)f_2(x-t)\,dt$$

$$= A_1A_2[\pi/(c_1+c_2)]^{0.5}\exp\{-[c_1c_2/(c_1+c_2)][x-(x_1-x_2)]^2\},$$

we obtain

$$Q_m(x) = w_Q \sum_{l=1}^{N} \sum_{k=1}^{N} A_lA_k \exp(-0.5 \cdot c[x-(x_l-x_k)]^2), \quad (10)$$

$$Q_{m1}(x) = w_Q \sum_{l=1}^{N} \sum_{k=1}^{N} A_l A_k \exp(-0.5 \cdot c[x - (x_l + x_k)]^2), \tag{11}$$

$$Q_{m2}(x) = w_Q \sum_{l=1}^{N} \sum_{k=1}^{N} A_l A_k \exp(-0.5 \cdot c[x + (x_l + x_k)]^2), \tag{12}$$

where w_Q is given by $w_Q = (\pi/2c)^{0.5}$.

Additional convolution with H_1 leads to

$$H_1 * Q_{m2} = w_Q w_{HQ} \sum_{l=1}^{N} \sum_{k=1}^{N} A_l A_k \exp\{-[c \cdot c_1/(c + 2c_1)][x + (x_l + x_k) - x_1]^2\}, \tag{13}$$

where $w_{HQ} = [c_1/(c_1 + 0.5c)]^{0.5}$.

APPENDIX B

Derivation of the Averaged Structure Factor $\overline{F_0^2}$

We choose as origin of the system the centre between $\rho_m(x)$ and $\rho_{-m}(x)$. We denote the deviation of l_1 from its mean value by a. The spacing between two symmetrically arranged Gaussian peaks is then $2x_k + a$. By the well-known Fourier transform of a Gaussian function, F_0^2 is given by

$$\begin{aligned} F_0^2(b) &= u_0^2 \left[\sum_{k=1}^{N} 2A_k \cos 2\pi b x_k\right]^2 \\ &= 2u_0^2 \left\{\sum_{k=1}^{N} A_k^2(1 + \cos 4\pi b x_k) + \sum_{k=1}^{N} \sum_{m=k+1}^{N} A_k A_m 2[\cos 2\pi b(x_k + x_m) \right. \\ &\quad \left. + \cos 2\pi b(x_k - x_m)]\right\}, \end{aligned} \tag{14}$$

where u_0 is given by $u_0 = (\pi/c)^{0.5} \exp(-\pi^2 b^2/c)$.

Replacing x_k by $x_k + a/2$, multiplying by $H_1(a)$, and integrating with respect to a, we obtain

$$\begin{aligned} \overline{F_0^2}(b) &= 2u_0^2 \left\{\sum_{k=1}^{N} A_k^2(1 + u_1 \cos 4\pi b x_k) \right. \\ &\quad \left. + \sum_{k=1}^{N} \sum_{m=k+1}^{N} A_k A_m[\cos 2\pi b(x_k - x_m) + u_1 \cos 2\pi b(x_k + x_m)]\right\}, \end{aligned} \tag{15}$$

where u_1 is given by $u_1(b) = \exp(-\pi^2 b^2/c_1)$.

APPENDIX C

Modified Beam Height Collimation Correction

In the case of a partial orientation of stacked ghosts, a modified beam height correction is necessary.

The commonly used collimation corrections are related to isotropic scattering curves (see, for example, Lake, 1967). If the other extreme situation is realized, a perfectly oriented system, a beam height correction is not required.

In the case of a mosaic spread, the scattering is limited to a defined arc on the Debye-Scherrer ring with an intensity distribution along this arc depending on the distribution function of the particle orientations.

We assume that this distribution function can be approximated by a Gaussian function (normal distribution), centered about the preferred orientation axis.

Starting with the well-known smearing integral (only height smearing is considered, using the iterative procedure of Lake [1967])

$$I(b) = \int_{-\infty}^{+\infty} W_z(z) I_0[(b^2 + z^2)^{1/2}]\,dz, \tag{16}$$

where $I(b)$ = height smeared intensity function; $I_0(b)$ = "true" intensity function (desmeared intensity); $W_z(z)$ = primary beam height weighting function.

An additional condition on account of the mosaic spread must be introduced:

$$I(b) = \int_{-\infty}^{+\infty} W_z(z) \cdot H(z,b) \cdot I_0[(b^2 + z^2)^{1/2}]\,dz, \tag{17}$$

where $H(z, b)$ is related to the half angle of divergence of the disorientation as follows:

$$H(z,b) = \exp[-c(b) \cdot z^2]. \tag{18}$$

At each point b on the film only that part of the primary beam contributes to the scattering which lies within the arc of mosaic spread. Denoting the value at half width of $H(z, b)$ by z_0, we get $H(z_0, b) = \exp[-c(b) \cdot z_0^2] = 0.5$, and considering the rectangular triangle

$$\tan \alpha = z_0/b, \tag{19}$$

we obtain

$$H(z,b) = \exp[-0.69 \cdot z^2/(b^2 \cdot \tan^2 \alpha)] \tag{20}$$

In the preceding case, α was estimated at 30°.

Thus, in the iterative procedure (Lake, 1967), for each value of b the corresponding function $H(z, b)$ has been calculated and used in the smearing integral.

Several tests have been made to control the effect of the angle of disorientation.

It has been found that the resulting desmeared curve $I(b)$ is only slightly influenced by a variation of $\tan \alpha$ within the range of $\pm 20\%$.

A constant factor was introduced to compare the resulting curve after "arc desmearing" with the scattering curve observed using pointlike collimation (Fig. 8).

REFERENCES

BLAUROCK, A. E., and W. R. LIEB. 1975. X-ray diffraction studies of biomembranes. *Nature (Lond.).* **255:** 370.

BLAUROCK, A. E., and J. C. NELANDER. 1976. Disorder in nerve myelin. Analysis of the diffuse X-ray scattering. *J. Mol. Biol.* **103:**421.

BRAMLEY, T. A., and R. COLEMAN. 1972. Effects of inclusion of Ca^{2+}, Mg^{2+}, EDTA or EGTA during the preparation of erythrocyte ghosts by hypotonic haemolysis. *Biochim. Biophys. Acta.* **290:**219.

BRETSCHER, M. S. 1973. Membrane structure: some general principles. *Science (Wash. D.C.).* **181**:622.

DODGE, J. R., C. MITCHELL, and D. J. HANAHAN. 1963. The preparation and chemical characteristics of hemoglobin-free ghosts of human erythrocytes. *Arch. Biochem. Biophys.* **100**:119.

FINEAN, J. B., R. COLEMAN, W. G. GREEN, and A. R. LIMBRICK. 1966. Low angle X-ray diffraction and electron-microscope studies of isolated cell membranes. *J. Cell Sci.* **1**:287.

FINEAN, J. B., R. COLEMAN, S. KNUTTON, A. R. LIMBRICK, and J. E. THOMPSON. 1968. Structural studies of cell membrane preparations. *J. Gen. Physiol.* **51**:19*s*.

FINEAN, J. B. 1972. X-ray diffraction studies of isolated cell membrane preparations. *Chem. Phys. Lipids.* **8**:279.

HOSEMANN, R., and S. N. BAGCHI. 1962. Direct analysis of diffraction by matter. North-Holland Publishing Company, Amsterdam. 121.

HUSSON, F., and V. LUZZATI. 1963. Structure of red cell ghosts and the effect of saponin treatment. *Nature (Lond.).* **197**:822.

KNUTTON, S., J. B. FINEAN, R. COLEMAN, and A. R. LIMBRICK. 1970. Low angle X-ray diffraction and electron-microscope studies of isolated erythrocyte membranes. *J. Cell Sci.* **7**:357.

KREUTZ, W. 1968. Röntgenographische Strukturuntersuchungen der Photosynthese-Membran. Habilitationsschrift D 83, Technische Universität, Berlin, W. Germany. 14.

KREUTZ, W. 1970. X-ray structure research on the photosynthetic membrane. *Adv. Bot. Res.* **3**:53.

KREUTZ, W., and E. H. PAPE. 1975. Evaluation of X-ray diffraction patterns of biomembrane systems. *In* Summer Institute on the Physics of Biological Membranes. K. Colbow, editor. Simon Fraser University, Vancouver, B.C., Canada. 378.

LAKE, J. A. 1967. An iterative method of slit-correcting small angle X-ray data. *Acta Cryst.* **23**:191.

LESSLAUER, W., J. CAIN, and J. K. BLASIE. 1971. On the location of 1-anilino-8-naphtalene sulfonate (ANS) in lipid model systems: an X-ray diffraction study. *Biochim. Biophys. Acta.* **241**:247.

LESSLAUER, W., and J. K. BLASIE. 1972. Direct determination of the structure of barium stearate multilayers by x-ray diffraction. *Biophys. J.* **12**:175.

MARQUARDT, D. W. 1963. An algorithm for least-squares estimation of nonlinear parameters. *J. Soc. Indust. Appl. Math.* **11**:431.

MCINTOSH, T. J., and C. R. WORTHINGTON. 1974. Direct determination of the lamellar structure of peripheral nerve myelin at low resolution (17 Å). *Biophys. J.* **14**:363.

MCMILLAN, P. N., and R. B. LUFTIG. 1975. Preservation of membrane ultrastructure with aldehyde or imidate fixatives. *J. Ultrastruct. Res.* **52**:243.

PAPE, E. H. 1974. X-ray small angle scattering. A new deconvolution method for evaluating electron density distribution from small angle scattering diagrams. *Biophys. J.* **14**:284.

PAPE, E. H., W. MENKE, D. WEICK, and R. HOSEMANN. 1974. Small angle X-ray scattering of the thylacoid membranes of *Rhodopseudomonas spheroides* in aqueous suspensions. *Biophys. J.* **14**:221.

SCHNEIDER, W., U. FEINE, F. SCHUNTER, K. STREIER. 1972. Verlängerung der Überlebenszeit gewaschener Erythrozytensedimente in vivo durch die Wahl einer adäquaten Waschlösung. *Med. Welt.* **23**:368.

SCHWARTZ, S., J. E. CAIN, E. A. DRATZ, and J. K. BLASIE. 1975. An analysis of lamellar X-ray diffraction from disordered membrane multilayers with application to data from retinal rod outer segments. *Biophys. J.* **15**:1201.

STAMATOFF, J. B., S. KRIMM, and N. R. HARVIE. 1975. X-ray diffraction studies of human erythrocyte membrane structure. *Proc. Natl. Acad. Sci. U.S.A.* **72**:531.

STECK, T. L. 1974. The organization of proteins in the human red blood cell membrane. A review. *J. Cell Biol.* **62**:1.

TILNEY, L. G., and P. DETMERS. 1975. Actin in erythrocyte ghosts and its association with spectrin. Evidence for a non-filamentous form of these two molecules in situ. *J. Cell Biol.* **66**:508.

VAINSHTEIN, B. K. 1966. Diffraction of X-rays by chain molecules. Elsevier Scientific Publishing Company, Amsterdam. 216.

WEICK, D. 1974. Note on the theory of X-ray diffraction by spherical shell structures. *Biophys. J.* **14**:233.

WILKINS, M. H. F., BLAUROCK, A. E., and D. M. ENGELMAN. 1971. Bilayer structure in membranes. *Nat. New Biol.* **230**:72.

WORTHINGTON, C. R., and T. J. MCINTOSH. 1974. Direct determination of the lamellar structure of peripheral nerve myelin at moderate resolution (7 Å). *Biophys. J.* **14**:703.

ZWAAL, R. F. A., B. ROELOFSEN, and C. M. COLLEY. 1973. Localization of red cell membrane constituents. *Biochim. Biophys. Acta.* **300**:159.